Journal of Theoretical Medicine, 2002 Vol. 4 (1), pp. 67–74

Taylor & Francis
healthsciences

Automatic Recognition of Muscle-invasive T-lymphocytes Expressing Dipeptidyl-peptidase IV (CD26) and Analysis of the Associated Cell Surface Phenotypes

W. SCHUBERT[a,b,*], M. FRIEDENBERGER[a], R. HAARS[a], M. BODE[b], L. PHILIPSEN[b], T. NATTKEMPER[c] and H. RITTER[c]

[a]*Institute of Medical Neurobiology, Molecular pattern recognition research group, Otto-von-Guericke University of Magdeburg, ZENIT-Building, Leipziger Str. 44, 39120 Magdeburg, Germany;* [b]*MELTEC Ltd., ZENIT-Building, Leipziger Str. 44, 39120 Magdeburg, Germany;* [c]*Neuroinformatics group, University of Bielefeld, 33619 Bielefeld, Germany*

(Received 1 August 2000; In final form 23 April 2001)

A neural cell detection system (NCDS) for the automatic quantitation of fluorescent lymphocytes in tissue sections was used to analyze CD26 expression in muscle-invasive T-cells. CD26 is a cell surface dipeptidyl-peptidase IV (DPP IV) involved in co-stimulatory activation of T-cells and also in adhesive events. The NCDS system acquires visual knowledge from a set of training cell image patches selected by a user. The trained system evaluates an image in 2 min calculating (i) the number, (ii) the positions and (iii) the phenotypes of the fluorescent cells. In the present study we have used the NCDS to identity DPP IV (CD26) expressing invasive lymphocytes in sarcoid myopathy and to analyze the associated cell surface phenotypes. We find highly unusual phenotypes characterized by differential combination of seven cell surface receptors usually involved in co-stimulatory events in T-lymphocytes. The data support a differential adhesive rather than a co-stimulatory role of CD26 in muscle-invasive cells. The adaptability of the NCDS algorithm to diverse types of cells should enable us to approach any invasion process, including invasion of malignant cells.

Keywords: Muscle; CD26; Neural network; Image analysis; Inflammatory myopathy

1. INTRODUCTION

Dipeptidyl-peptidase IV (DPP IV, CD26) is a cell surface transmembrane protein characterized by a short N-terminal cytoplasmic domain and a long extra cellular region with a sugar rich and a Cys-rich domain. A third 260 aminoacid C-terminal extra cellular region was found to exhibit DPP IV enzyme catalytic activity, (Hegen *et al.*, 1990; Darmoul *et al.*, 1992; Tanaka *et al.*, 1992). DPP IV is a member of the prolyl oligopeptidase family which is defined by the requirement of the catalytic triad in the unique order Ser, Asp, His (Abbott *et al.*, 1994). The enzyme cleaves amino-terminal dipeptides with either L-proline or L-alanine in the penultimate position.

DPP IV has been shown to be expressed by a variety of cell types including T- and B-lymphocytes, activated NK cells, and by epithelia of the intestine, the prostate, and the proximal tubuli of kidneys (Stein *et al.*, 1989; Hegen *et al.*, 1990; Bühling *et al.*, 1995). DPP IV is implicated in inflammatory processes and appears to play a part in the progression of certain malignant tumors (Morrison *et al.*, 1993; Iwata and Morimoto, 1999). Given the cellular immune response (Morimoto and Schlossman, 1998), an important function of DPP IV is its role as a co-stimulatory cell surface protein that is involved in the activation of the T-lymphocyte.

Within the T-cell activation cascade, antibody-induced stimulation of DPP IV leads to tyrosine phosphorylation of several intracellular proteins with a similar pattern to that seen after stimulation of the T-cell antigen receptor (TCR)/CD3 complex of CD4- or CD8-expressing T-cells (Hegen *et al.*, 1997). Given stimulation of T-cells via this complex, CD26 provides a true co-stimulatory function that can up-regulate the signal-transducing properties of the TCR.

*Corresponding author. Address: Institute of Medical Neurobiology, Molecular pattern recognition research group, Otto-von-Guericke University of Magdeburg, ZENIT-Building, Leipziger Str. 44, 39120 Magdeburg, Germany. Tel.: +49-391-6117-174. Fax: +49-391-6117-176. E-mail: schubert@pc.mdlink.de

ISSN 1027-3662
DOI: 10.1080/10273660290015189

TABLE I CD cell surface antigen analyzed in this study

CD antigen	Specificity	Monoclonal antibody clone
CD 26	DPP IV; adhesive deaminase binding protein	L272
CD 8	Co-recognition receptor for MHC class I with TCR	B9.11
CD 4	Co-recognition receptor for MHC class II with TCR	13B8.2
CD 11 b	α M integrin chain of MAC-1 complex, C3bi receptor "CR3"	44
CD 19	Receptor of the Slg family, modulates B cell responsiveness	J.4.119
CD 2	SRBC receptor, ligand for LFA 3 (CD58)	39C1.5
CD 3	Signal transduction receptor complex associated with TCR	UCHT1

In peripheral blood the T-lymphocytes that express DPP IV are either CD4 or CD8 positive cells, and, as a rule show co-expression of intact TCR/CD3 complexes. Hence a T-cell that can be co-stimulated via CD26 is a $CD4^+/CD3^+/TCR^+/CD26^+$, or a $CD8^+/CD3^+/TCR^+/CD26^+$ T-cell. In addition, the majority of these T-cells also express CD2, which can provide an alternative pathway of T-cell activation (Davis *et al.*, 1998).

In the present paper we have addressed the expression of DPP IV and DPP IV-associated cell surface phenotypes in muscle-invasive T-lymphocytes. Multi-epitope imaging microscopy (Schubert, 1992) was used to co-localize seven different cell surface proteins including CD26 on the cell surface of these muscle-invasive T-cells. The latter technology was coupled to a new learning algorithm (Nattkemper *et al.*, 1999, 2000a), which automatically recognizes T-cells within tissue sections obtained from patients suffering from chronic inflammatory muscle disease. We have selected chronic sarcoid myopathy, which represents a human disease type showing T-lymphocyte invasion of the muscle tissue. The T-lymphocytes are present to a large extent within the connective tissue between the muscle fiber fascicles, a space that is defined as the perimysium. In addition, sarcoid myopathy is characterized by the formation of giant cells, that is supposed to be driven by the cooperation between T-cells and macrophages (Wahlstrom *et al.*, 1999).

In the present study we have examined whether muscle-invasive T-lymphocytes exhibit a cell surface phenotype required for T-cell activation and CD26-associated T-cell stimulation. Using a library of seven different monoclonal antibodies we find that the majority of the T-cells do not co-express the cell surface receptor sets, which would be required for T-cell activation via the co-stimulator molecule CD26. Instead these T-cells express unusual cell surface phenotypes by heterogeneous receptor combinations, most of which are minus-variants of the phenotypes found in the blood. We suggest that these "unusual" cell surface phenotypes are involved in differential adhesion mechanisms and T-cell migration rather than T-cell activation.

We also describe a learning algorithm, by which T-cells within the tissue can be automatically recognized and quantified. Given that a large number of tissue sections have to be mapped by multi-epitope imaging, the algorithm opens the possibility for high-throughput screening of invasive lymphocytes in tissues (Nattkemper *et al.*, 2000a). The adaptability of the algorithm to diverse types of cells should enable us to approach any invasion process, including invasion of malignant cells.

2. IMAGING METHODS

In order to address the CD26-associated phenotype of muscle-invasive T-cells, we have applied seven monoclonal antibodies directed against cell surface antigens (CD antigens) in cryosections of diagnostic biopsies. The antigens are listed in Table I. All antibodies were directly conjugated to dyes and applied to the tissue sections as described earlier (Schubert, 1992). Each fluorescent signal was recorded as a digitized image by a cooled CCD camera. Fluorescent cells were either localized by medical experts using a mouse-delineation of the fluorescent area, or were automatically recognized by the learning algorithm described below.

3. AUTOMATIC T-CELL FLUORESCENCE PATTERN RECOGNITION

To identify CD26 positive T-cells and other T-cell types in tissue sections we used a modular computer system that detects the positions of up to 95% of all fluorescent lymphocytes in one given input image M, the digitized fluorescence micrograph (Nattkemper *et al.*, 1999). The first module of the cell detection system is a trained cell classifier that classifies a square image region p of 15×15 pixels to a so called evidence value $C(p) \in [0; 1]$ representing the probability that the center of p is occupied by a fluorescent cell. The second module evaluates the evidence values of all points in M to a list of positions of fluorescent lymphocytes. The positions of the detected cells are visualized on a screen and stored in a database. In the following subsections we describe the cell detection system briefly, see (Nattkemper *et al.*, 1999, 2000b) for details.

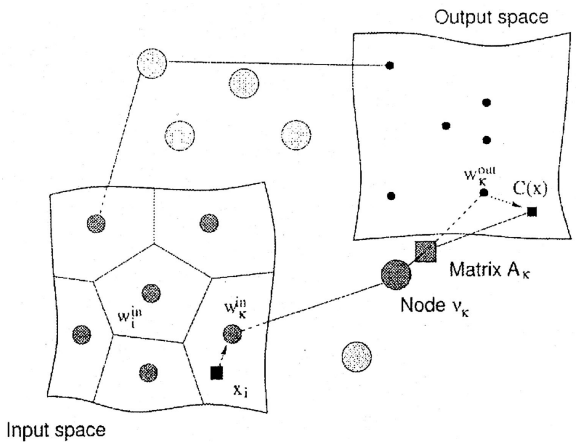

FIGURE 1 Example illustrating a Local Linear Map (LLM) approximating a mapping with six nodes. The LLM's nodes w_i^{in} form Voroni cells of the input space. The mapping into the output space is performed by a local linear transformation given by A_k and w_k^{out}. First, the nearest neighbor w_k^{in} to the input is selected, then the input is mapped via the coupled matrix A_k.

4. TRAINING OF THE CELL CLASSIFIER

The cell classifier $C(p)$ is a trained artificial neural network (ANN). Neural networks have been shown to be powerful classification tools in many industrial computer vision applications. In biomedical image analysis the application of ANNs is not frequent, and only recently applications have been published (Sjoestroem *et al.*, 1999).

To map an image region p to its evidence value, six numerical feature values are calculated for p and combined to a so called feature vector $x \in IR^6$. Here the term "vector" describes a set of numerical elements as used in the field of computational pattern recognition. The computation of the feature vector is described in 12. The trained ANN computes the evidence value for p by mapping its feature vector $\mathbf{x}$ to $C(\mathbf{x})$ using the learned classification mappings $C : IR^6 \mapsto IR$.

The ANN used for cell classification is of Local Linear Map-type (LLM) which was introduced by Ritter (1991) and has been shown to be a powerful tool in fast learning of non-linear mappings,

$$C : IR^{d_{\text{in}}} \mapsto IR^{d_{\text{out}}},$$

such as classification tasks in Computer Vision applications (Heidemann and Ritter, 1999). The LLM-approach was originally motivated by the Kohonen Self-organizing Map (Kohonen, 1989) with the aim to obtain a good map resolution even with a small number of units. In the LLM learning scheme unsupervised and supervised learning are combined in contrast to the widely used multi-layer perception trained with back-propagation (Rummelhart *et al.*, 1986). The LLM is given through

$$\left\{w_i^{\text{in}} \in IR^{d_{\text{in}}}, w_i^{\text{out}} \in IR^{d_{\text{out}}}, A_1 \in IR^{d_{\text{in}} x d_{\text{out}}}, i = 1 \ldots n\right\}$$

and a triple

$$v_i = \left(w_i^{\text{in}}, w_i^{\text{out}}, A_i\right)$$

is called node. In the present work the LLM parameters are $d_{\text{in}} = 6$, $d_{\text{out}} = 1$, $n = 25$.

By calculating

$$C(x) = w_k^{\text{out}} + A_k\left(x - w_k^{\text{in}}\right)$$

the input feature vector $\mathbf{x}$ is mapped to the evidence value $C(x)$. k holds

$$k = \arg\min\left\{\|x - w_i^{\text{in}}\|\right\},$$

so w_k^{in} is the nearest neighbor to input $\mathbf{x}$. An illustration is given in Fig. 1.

The three free parameters of each of the n nodes

$$\left(w_i^{\text{in}}, w_i^{\text{out}}, A_i, i = i \ldots n\right)$$

are trained with a pre-selected set Γ of m (input, output)-pairs,

$$\Gamma = \{(x_\alpha, y_\alpha)\}, \alpha = 1 \ldots m$$

that is composed of two subsets $\Gamma = \Gamma^{\text{pos}} \cup \Gamma^{\text{neg}}$. The so called positive set

$$\Gamma^{\text{pos}} = \left\{\left(x_\alpha^{\text{pos}}, 1\right)\right\}$$

consists of feature vectors x_α^{pos} computed (see below) from image patches centered at positive training samples for fluorescent cells, together with the target output value

$$y_\alpha^{\text{pos}} = C\left(x_\alpha^{\text{pos}}\right) = 1$$

of the classifier. The negative set

$$\Gamma^{\text{neg}} = \left\{\left(x_\alpha^{\text{neg}}, 0\right)\right\}$$

consists of feature vectors x_α^{neg} computed from non-cell image patches (see below) and their target classification output value

$$y_\alpha^{\text{neg}} = C\left(x_\alpha^{\text{neg}}\right) = 0.$$

To obtain 15×15 sized image patches for computing, the feature vectors $x_\alpha^{\text{pos}} \in \Gamma^{\text{pos}}$ are an interactive program displaying the digitized microscope fluorescence images and allowing users to select cell centers with the aid of a mouse cursor. The set Γ^{neg} is then generated automatically by randomly selecting image points in a minimum distance of $r_{\text{neg}} = 5$ pixels from any of the selected cells of Γ^{pos}. For each of these randomly selected points a feature vector x_α^{neg} is computed by the same procedure as for Γ^{pos}. In one training step of the LLM first one input–output pair (x_α, y_α) is selected randomly from the training set $\Gamma = \{(x_\alpha, y_\alpha)\}$, secondly the best-match node v_k is found, and third its weights are changed according to the

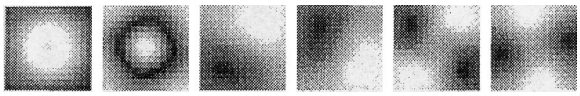

FIGURE 2 Eigencells calculated from manual mouse-click selection of 120 cross-sectioned lymphocytes.

following learning rules

$$\Delta w_k^{\text{in}} = \varepsilon^{\text{in}}\left(x_a - w_k^{\text{in}}\right) \tag{1}$$

$$\Delta w_k^{\text{out}} = \varepsilon^{\text{out}}(y_\alpha - C(x_\alpha)) + A_k \Delta w_k^{\text{in}} \tag{2}$$

$$\Delta A_k = \varepsilon^{\text{A}}(y_\alpha - C(x_\alpha)) \frac{\left(x_\alpha - w_k^{\text{in}}\right)^{\text{T}}}{\|x_\alpha - w_k^{\text{in}}\|^2} \tag{3}$$

with ε^{in}, ε^{out}, $\varepsilon^{\text{A}} \in [0, 1]$ as exponentially decreasing learning step sizes. Looking at the rules, one can observe that learning rule (1) is an online version of k-means (Moody and Darken, 1989) for positioning the n centers of w_i^{in}, And (2) and (3) adjust a linear mapping specified by vector w_{ki}^{out} and matrix A_k in the vincinity (Voroni cell) around the best match node.

5. CALCULATION OF CELL FEATURES

In the development of a classification system a suitable feature computation is crucial for the performance of the system. In the context of this work the cell features should be robust against small changes of size, intensity and curvature of the fluorescent cells in the 15 × 15 patches.

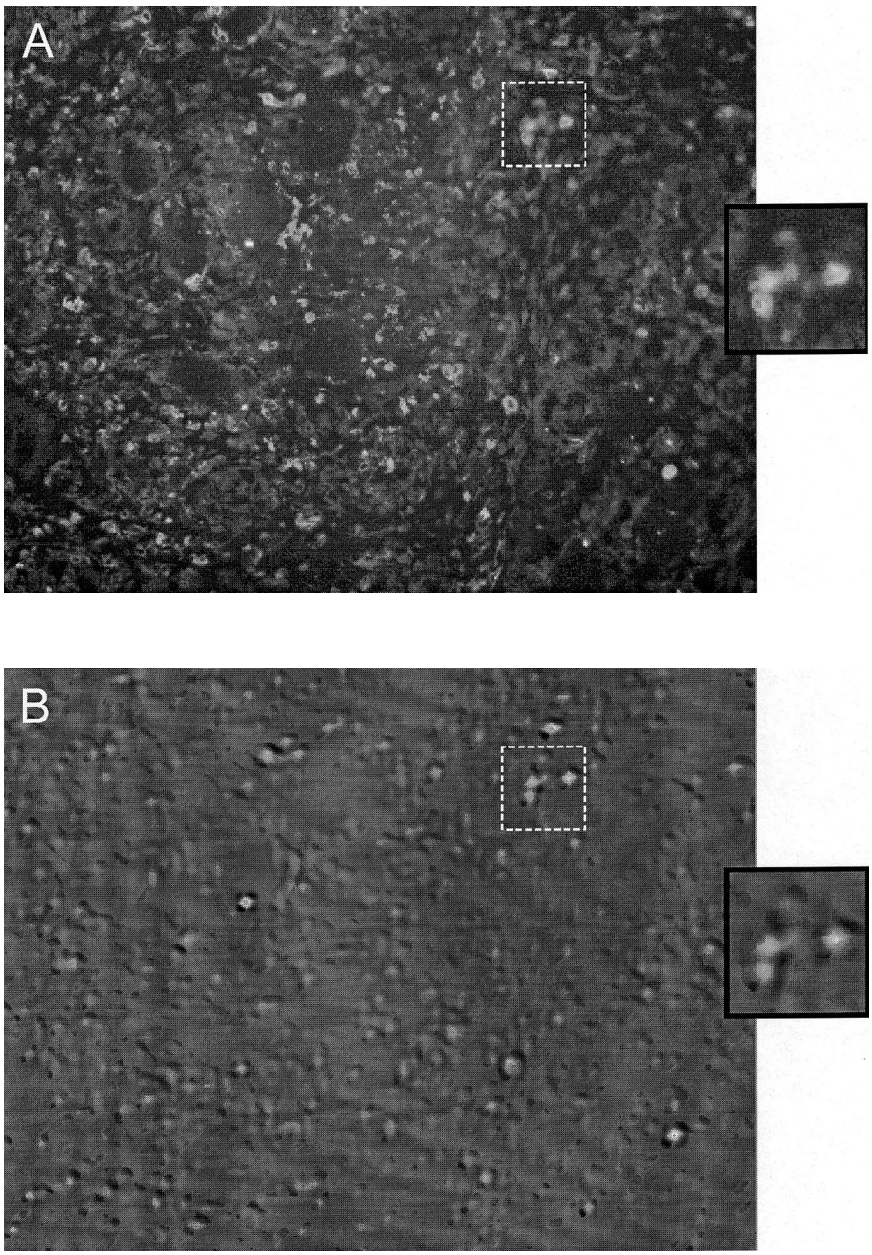

FIGURE 3 (*caption opposite*)

TABLE II Simultaneous detection of 24 T-cell phenotypes expressed different combinations of seven different cell surface receptors

	Combinatorial phenotype						
Frequency (%) of T-cell in muscle	CD2	CD3	CD4	CD8	CD11b	CD19	CD26
35.1	0	0	1	0	0	0	0
29.9	1	0	0	0	0	0	0
15.2	1	0	1	0	0	0	0
5.0	1	1	1	0	0	0	0
3.1	1	0	0	0	1	0	0
2.0	0	0	0	0	1	0	0
1.8	1	0	0	1	0	0	0
1.5	1	1	0	1	0	0	0
1.3	1	1	0	1	0	0	1
1.3	1	1	1	0	0	0	1
1.1	0	0	0	0	0	1	0
0.9	1	0	1	1	0	0	0
0.9	1	0	1	1	0	0	1
0.7	1	1	0	0	0	0	0
0.7	0	1	1	0	0	0	0
0.7	0	0	1	0	1	0	0
0.6	1	0	0	0	0	0	1
0.4	1	1	1	1	0	0	0
0.4	0	0	1	0	0	0	1
0.4	1	0	0	0	1	0	1
0.2	1	0	1	0	1	0	1
0.2	1	0	0	0	0	1	0
0.2	1	0	0	1	0	0	1
0.2	0	0	1	1	0	0	1

Because the cells are in muscle tissue, their size, intensity and shape show considerable variation. One way to map an image point p to a feature vector $x \in IR^6$ is to calculate the overlaps of a surrounding image region of size 15×15 with a set of 6 filters, such as Gabor filters (Dunn *et al.*, 1994; Lee, 1996) or steerable derivatives of 2-dimensional Gaussians (Rao and Ballard, 1995). The disadvantage of such filters is that they contain several parameters (radius, orientations, etc.), which have to be fitted according to the particular application. This is difficult and/or time- consuming for a non-expert user. To avoid such problems we use here a Principal Component Analysis (PCA) on a set of 15×15-sized image patches of centered cells, which is a data-driven approach.

In this application the PCA-technique uses 6 eigenvectors $u_\lambda \in IR^{N^2}$ (so called "eigencells") of the

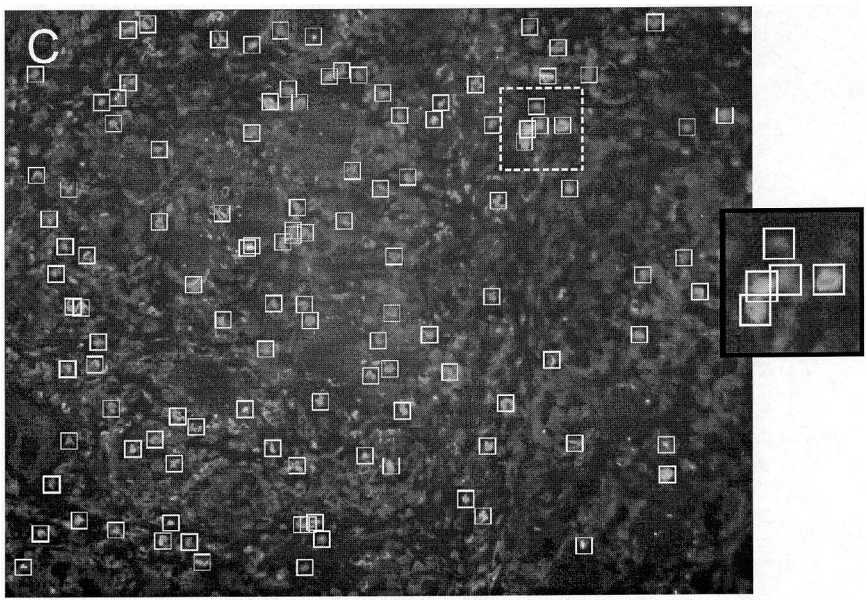

FIGURE 3 The detection of CD26 fluorescent lymphocytes in muscle tissue is illustrated. Figure 3A shows the input image of invading lymphocytes in muscle tissue. The cells were immunolabeled with anti-CD26. The evidence map computed by the LLM is illustrated in Fig. 3B. The evidence values are scaled to [0;255] for visualization purposes. A high value stands for a high evidence of a fluorescent cell. The finally detected positions of fluorescent cells as indicated by white boxes are shown in Fig. 3C. A typical image showing five lymphocytes is shown in the inset on the right hand side of each picture.

covariance matrix of 15 × 15 image patches. The patches are the 15 × 15-sized image regions around the handselected image points of fluorescent cells which were selected for training (see above). The usage of such eigenvectors is a well-known technique for detection tasks (Turk and Pentland, 1991; Varchim *et al.*, 1997). A listing of the eigenvalues in descending order reveals that the majority of the variance in the image data is described by the six eigencells of the six highest eigenvalues. Figure 2 shows 6 eigencells computed from the training set. These are taken to generate the 6-dimensional feature vector **x** for an image point by scalar multiplication of its 15 × 15 neighborhood with the six eigencells.

6. CELL DETECTION IN FLUORESCENCE MICROGRAPHS WITH THE LLM

For the full automatic detection of CD26 positive cells and other T-cell types in one given micrograph every image point p is mapped to its evidence value [0,1] by calculating the LLM output $C(x) \in [0, 1]$ for its feature vector **x** of its surrounding 15 × 15-image patch. Mapping evidences of all points to their corresponding image positions we achieve the so-called evidence map. A point p_e, in the evidence map, which has the highest evidence value $C(x)$ within a 5-pixel radius above a given evidence threshold $t_e = 0.5$, is the result position of the center of one fluorescent cell, so $C(x)$ obeys

$$C(p) > 0.5 \wedge C(p) = \arg\max\{C(p')\} \quad d(p', p) < 5$$

One input micrograph (A), its evidence map (B) and the detected fluorescent cells (C) are shown in Fig. 3.

7. RESULTS AND DISCUSSION

In the present paper we have analyzed invasive T-lymphocytes in muscle tissue for the expression of DPP IV (CD26). To analyze the cell surface receptor expression patterns of these T-cells we used the multi-epitope imaging approach (Schubert, 1992), in a new form working at the level of single clearly identifiable cells (details will be published elsewhere). Here we used a limited number of seven monoclonal antibodies to simultaneously detect seven different T-cell surface proteins. By this approach we have addressed the role of CD26 as a co-stimulatory molecule in the T-cell activation cascade, in order to examine, whether muscle-invasive T-cells in sarcoid myopathy do or do not show the expected CD26- associated patterns of receptor expression. This study extends the data obtained by the analysis of lymphocyte associated proteins found to be expressed in muscle tissue (Schubert *et al.*, 1989, 1993; Schubert, 1991; Haars *et al.*, 2000).

The muscle-invasive T-cells were found to be present as low-density infiltrates in the perymysium of the muscle tissue. Surprisingly, the majority of these cells were negative for CD26, indicating that activation of T-cells via the CD26 dependent pathway does not play a key role in this disease. $CD19^+$ B-lymphocytes were rare and these did not express CD26. Together, only 5, 4% of the T-cells expressed CD26 (see Table II). These cells showed substantial variation according to differential expression of the six other cell surface receptors (CD2, CD3, CD4, CD8, CD11b). Among the CD26-positive cell fraction, the co-expression of CD3 and CD4 or CD8 and CD3 was seen most frequently, whilst few CD26-positive cells showed co-expression of CD4 or CD8 alone. An unusual T-cell type was seen which shows co-expression of CD2, CD1lb and CD2.6, whilst CD4, CD8 and CD3 were absent in these cells. Finally the vast majority of T-cells, which were negative for CD26 (~95%) also showed a highly unusual phenotype characterized either by expression of CD4 alone, or CD2 alone, whilst co-expression of the CD3 receptor complex was restricted to only a minor fraction of CD4-positive and CD8-positive T-lymphocytes (for summary see Table II).

Together these data show, that muscle-invasive T-lymphocytes in sarcoid myopathy show a highly unusual phenotype at two levels: First, T-lymphocytes in the peripheral blood, that express CD26, are CD4-positive or CD8-positive T-cells which are also characterized by co-expression of the CD3 complex, as a rule, and most of these T-cells also show co-expression of CD2, which is implicated in an alternative pathway of T-cell activation (Davis *et al.*, 1998). In the present study it is shown that within the minor fraction of muscle-invasive T-cells, which show the expression of CD26 (5, 6% of all cells), only approximately one half of these cells do show the CD2/CD3/CD4/CD26 or the CD2/CD3/CD8/CD26 phenotype as expected for a fully "equipped" T-cell. The other half of the CD26-positive cells express minus-variants of this pattern, characterized by omission of one or more of the CD3/CD2/CD8 or CD4 receptors. Interestingly, in these cells, CD26 may occur together with the α M integrin CD11b. It is unclear at present, whether the latter cells are T-cells or macrophages. Together, a fraction of the muscle-invasive T-cells show both cell surfaces that are compatible and others that are not compatible with a role of CD26 as a co-stimulatory signal of T-cell activation.

Second, the majority of T-cells, that have invaded the muscle tissue in sarcoid myopathy are clear-cut minus-variants of the T-cell surface expression patterns normally found in the blood, because these cells *in situ* only express either CD4 or CD2 (together 64% of all invasive T-cells), whilst CD3, CD8, CD11b and CD26 are absent. Another T-cell fraction, which is substantially less frequent is the $CD2^+/CD4^+$ (15%) and the $CD2^+/CD3^+/CD4^-$ T-cell type (5%). Only the latter- one would reflect the "normal" cell surface expression pattern of a CD4 T-cell. This demonstrates the predominant presence of T-cells, which, as a rule, lack receptor patterns at the cell surface, which would be obligatory for the T-cell activation

cascade. Hence, it is very unlikely that T-cells invading the muscle tissue in sarcoid myopathy undergo T-cell activation via the known battery of co-stimulatory receptors.

Alternatively we would like to suggest, that the heterogeneous "unusual" combinatorial receptor phenotypes of the T-cell surface are involved in differential adhesive functions and migratory mechanisms. This view is supported by the fact, that CD26, besides its role as a co-stimulatory signal in T-cell activation, also exerts adhesive functions by binding to collagen (Dang *et al.*, 1990). Adhesive functions have also been assigned to CD2, CD8, CD4 and CD11b (Barclay *et al.*, 1993; Pigott and Power, 1993). We therefore suggest, that all phenotypes detected in muscle tissue in our present study (Table II) are implicated in cell surface "decision-processes" that either fix the T-cell at a certain position in the tissue or promote T-cell migration. The T-cell may acquire this function by differentially combining receptors in a manner illustrated by the data presented in Table II.

The neural classifier used in the present study enables us to analyze $CD26^+$ and $CD26^-$ T-cell phenotypes at a large scale. The disease-associated phenotypic data presented here and the NCDS as a high-throughput approach could provide important links for mathematical modeling T-cell invasion at an integrated molecular and cellular level.

Acknowledgements

We thank F. Wedler for help in preparing the manuscript. The excellent technical assistance of M. Möckel is greatly acknowledged. This work was supported by grants from DFG (SFB 387), Schu 627/8-2 and BMBF 01ZZ9510/07NBL04.

References

Abbott, C.A., Baker, E., Sutherland, G.R. and McCaughan, G.W. (1994) "Genomic organisation, exact localization, and tissue expression of the human CD26 (dipeptidyl peptidase IV) gene", *Immunogenetics* **40**, 331–338.

Barclay, A.N., Birkeland, M.L., Brown, II, M., Beyers, II, A.D., Davis, II, S.J., Somoza, II, C. and Williams, II, A.F. (1993) The Leucocyte Antigen, Facts Book (Academic Press, London).

Bühling, F., Junker, U., Reinhold, D., Neubert, K., Jäger, L. and Ansorge, S. (1995) "Functional role of CD26 on human B lymphocytes", *Immunol. Lett.* **45**, 47–51.

Dang, N.H., Torimoto, Y., Schlossman, S.F. and Morimoto, C. (1990) "Human helper T-cell activation: functional involvement of two district collages receptors 1 F7 and integrin familiy", *J. Exp. Med.* **172**, 649–652.

Darmoul, D., Lacasa, M., Baricalut, L., Marguet, D., Sapin, C., Trotot, P., Barbat, A. and Trugman, G. (1992) "Dipeptidyl peptidase IV (CD26) gene expression in enterocyte-like colon cancer cell lines HT-29 and Caco-2. Cloning of the complete human coding sequence and changes of dipeptidyl peptidase IV mRNA levels during cell differentiation", *J. Biol. Chem.* **267**, 2200–2208.

Davis, S.J., Ikemizu, S., Wild, M.K. and van der Merwe, P.A. (1998) "CD2 and the nature of protein interactions mediating cell–cell recognition", *Immunol. Rev.* **163**, 217–236.

Dunn, D., Higgins, W.E. and Wakeley, J. (1994) "Texture segmentation using 2d Gabor elementary functions", *IEEE Trans. Pattern Anal. Machine Intelligence* **16**, 130–149.

Haars, R., Schneider, A., Bode, M. and Schubert, W. (2000) "Secretion and differential localization of the proteolytic cleavage products Aβ40 and Aβ42 of the Alzheimer amyloid precursor protein in human fetal myogenic cells", *Eur. J. Cell. Biol.* **79**, 1–7.

Hegen, M., Niedobitck, G., Klein, C.E., Stein, H. and Fleischer, B. (1990) "The T-cell triggering molecule Tp103 is associated with dipeptidyl aminopeptidase IV activity", *J. Immunol.* **144**, 2908–2914.

Hegen, M., Kameoka, J., Dong, R.-P., Schlossman, S.F. and Morimoto, C. (1997) "Cross-linking of CD26 by antibody induces tyrosine phosphorylation and activation of mitogen-activated protein kinase", *Immunology* **90**, 257–264.

Heidemann, G. and Ritter, H. (1999) "Combining multiple neural nets for visual feature selection and classification", ICANN 99. Ninth International Conference on Artificial Neural Networks, pp 365–370.

Iwata, S. and Morimoto, C. (1999) "CD26/dipeptidyl peptidase IV in context. The different roles of a ectoenzyme in malignant transformation", *J. Exp. Med.* **190**, 301–306.

Kohonen, T. (1989) Self organization and Associative Memory (Springer, Berlin).

Lee, T.S. (1996) "Image representation using 2d Gabor wavelets", *IEEE Trans. Pattern Anal. Machine Intelligence* **18**, 959–971.

Moody, J. and Darken, C. (1989) "Fast learning in networks of locally-tuned processing units", *Neural Comput.* **1**, 281–294.

Morimoto, C. and Schlossman, S.F. (1998) "The structure and function of CD26 in the T-cell immune response", *Immunol. Rev.* **161**, 55–70.

Morrison, M.E., Vijayasaradhi, S., Engelstein, D., Albino, A.P. and Houghton, A.N. (1993) "A marker for neoplastic progression of human melanocytes is a cell surface ectopeptidase", *J. Exp. Med.* **177**, 1135–1143.

Nattkemper, T.W., Ritter, H. and Schubert, W. (1999) "Extracting patterns of lymphocyte fluorescence from digital microscope images". *Intelligent Data Analysis in Medicine and Pharmacology 99 (IDAMAP), Workshop Notes*, Washington DC, USA. pp. 79–88

Nattkemper, T.W., Ritter, H. and Schubert, W. (2001) "A neural classifier enabling high-throughput topological analysis of lymphocytes in tissue sections", *IEE Transaction of Information Technology in Biomedicine* **5**, 138–149.

Nattkemper, T., Wersing, H., Schubert, W. and Ritter, H. (2000b) "A neural network architecture for automatic segmentation of fluorescence micrographs". *Proceedings of the Eighth European Symposium on Artificial Neural Network (ESANN)*, Bruges, Belgium.

Pigott, R. and Power, C. (1993) The Adhesion Molecule, Facts Book (Academic Press, London).

Rao, R. and Ballard, D (1995) "An active vision architecture based on iconic representations". Technical report, University of Rochester, CS.

Ritter, H. (1991) "Learning with the self-organizing map", In: Kohonen, T., ed, Artificial Neural Networks 1 (Elsevier Science Publishers, B.V., London).

Rummelhart, D., Hilton, G. and Williams, R. (1986) "Learning international representations by error propagation. Parallel distributed processing: explorations in the microstructure of cognition", *Foundations* **1**, 318–362.

Schubert, W. (1991) "Triple immunofluorescence confocal laser scanning microscopy: spatial correlation of novel cellular differentiation markers in human muscle biopsies", *Eur. J. Cell. Biol.* **55**, 272–285.

Schubert, W. (1992) "Antigenic determinants of T-lymphocyte αβ receptor and other leukocyte surface proteins as differential markers of skeletal muscle regeneration: detection of spatially and timely restricted pattern by MAM microscopy", *Eur. J. Cell. Biol.* **58**, 395–410.

Schubert, W., Zimmermann, K., Cramer, M. and Starzinski-Powitz, A. (1989) "Lymphocyte antigen Leu-19 as a molecular marker of regeneration in human skeletal muscle", *Proc. Natl Acad. Sci. USA* **86**, 307–311.

Schubert, W., Masters, C.L. and Beyreuther, K. (1993) "APP+ T-lymphocytes selectively sorted to endomysial tubes in polymyositis displace NCAM-expressing muscle fibers", *Eur. J. Cell. Biol.* **62**, 333–342.

Sjoestroem, P.J., Frydel, B.R. and Wahlberg, L.U. (1999) "Artifical neural network-aided image analysis system for cell counting", *Cytometry* **36**, 18–26.

Stein, H., Schwarting, R. and Niedobitek, G. (1989) In: Knapp, W., Dörken, B., Gilks, W.R., Rieber, E.P., Schmidt, R.E., Stein, H. and Kr. von dem Borne, A.E.G., eds, Leukocyte Typing IV (Oxford University Press, Oxford), pp 412–415.

Tanaka, T., Camerini, D., Seed, B., Torimoto, Y., Dang, N.H., Kemeoka, J., Dahlberg, H.N., Schlossman, S.F. and Morimoto, C. (1992) "Cloning and functional expression of the T-cell activation antigen CD 26", *J. Immunol.* **149**, 481–486.

Turk, M. and Pentland, A. (1991) "Eigenfaces for recognition", *J. Cognitive Neurosci.* **3**, 71–86.

Varchim, A.C.H., Rac, R. and Ritter, H. (1997) "Facial feature detection using neural networks", In: Wulfram Gestner, A., Germond, M.H. and Nicoud, J.-D., eds, Proceedings of the International Conference on Artificial Neural Network (Springer, Lausanne), pp 955–960.

Wahlstrom, J., Berlin, M., Skold, C.M., Wigzell, H., Eklund, A. and Grunewald, J. (1999) "Phenotypic analysis of lymphocytes and monocytes/macrophages in peripheral blood and bronchoalveolar lavage fluid from patients with pulmonary sarcoidosis", *Thorax* **54**, 339–346.